Proceedings of PVP2007
2007 ASME Pressure Vessels and Piping Division Conference
July 22-26, 2007, San Antonio, Texas

PVP2007-26193

THE EFFECT OF RESIDUAL STRESS AND MICROSTRUCTURE ON DISTORTION IN THIN WELDED STEEL PLATES

C. M. Davies
Dept. of Mechanical Engineering,
Imperial College London,
South Kensington Campus,
London, SW7 2AZ. UK.

R. C. Wimpory
Hahn-Meitner-Institut,
Glienicker Strasse 100,
D-14109, Berlin.
Germany.

M. Béreš
Dept. of Materials,
Imperial College London,
South Kensington Campus,
London, SW7 2AZ. UK.

M. P. Lightfoot
Marine Science and Technology,
University of Newcastle,
Newcastle Upon Tyne,
NE1 7RU. UK.

D. Dye
Dept. of Materials,
Imperial College London,
South Kensington Campus,
London, SW7 2AZ. UK.

E. Oliver
ISIS Facility,
Rutherford Appleton Laboratory,
Chilton,
Didcot, OX11 0QX. UK.

N. P. O'Dowd
Dept. of Mechanical and
Aeronautical Engineering,
University of Limerick,
Ireland.

G. J. Bruce
Marine Science and Technology,
University of Newcastle,
Newcastle Upon Tyne,
NE1 7RU. UK.

K. M. Nikbin
Dept. of Mechanical Engineering,
Imperial College London,
South Kensington Campus,
London, SW7 2AZ. UK.

ABSTRACT

The current trend in ship construction is to reduce the thickness of the ship panels, in order to minimize weight and maximize vessel speed. The ship panels of interest consist of 4 mm thick butt welded plates. This reduction in panel thickness may lead to excessive plate distortion during welding, resulting in significant additional costs during assembly. A ferritic-pearlitic DH-36 steel is used, in which phase transformations during welding may affect the distortion and stress states observed. Two large plates, representative of ship panels, have been butt welded using a metal inert gas (MIG) process. The temperature histories have been recorded during welding and the resulting distortion profile has been obtained using digital photography. Neutron diffraction measurements have been performed to determine the residual stress state in the plates before welding, due to e.g. processing and laser cutting, and after butt welding of the plates. Reference matchsticks from the weld, heat affected zone (HAZ) and parent plate have been taken from similar locations in nominally identical plates and measured to obtain the strain/stress free lattice parameter, a_0. A Rietveld analysis has been performed on the diffraction data. Post welding, hardness surveys have indicated the microstructural variation in the weld, parent plate and HAZ. Results from these on-going studies are presented which identify the key factors responsible for thin plate distortion.

Nomenclature

a, a_0	Lattice parameter, strain free lattice parameter
ν	Poisson's ratio
x, y, z	Co-ordinate axes
E	Elastic modulus
Q_1, Q_2	Scattering vectors
Å	Angstrom (1×10^{-10} metres)
θ_B	Bragg angle
ε	Strain
ε_1, ε_2, ε_3	Direct strains
σ	Stress
σ_1, σ_2, σ_3	Direct stresses

INTRODUCTION

Ship structures consist of panels constructed by butt welding large, thin plates, which range from 4 × 2 m to 8 × 3 m, with subsequent addition of fillet welded stiffeners. Current trends are to minimize plate thicknesses to 4 mm enabling a lightweight, high speed structure. The use of thin plates however, has been found to increase residual stresses severely in the plates following welding leading to large distortions. Such distortions subsequently cause difficulties in assembly and high rectification costs.

The overall aim of this work is to develop distortion prediction tools, using artificial neural networks (ANN), enabling the optimal fabrication process to be employed. Finite element (FE) models will be developed to simulate the welding process, including details of metallurgical changes that take place, and predict residual stresses, strains and distortions. Accurate finite element models, which require validation by experimental data, will then be used to train the ANN.

This paper reports the experimental studies performed on a butt welded sample. *In situ* thermal measurements have been obtained during the welding process. Neutron diffraction (ND) measurements have been performed to establish the residual stress state in the plate prior to welding, due to sheet rolling and laser cutting, and after the welding process. Metallographic investigations and hardness studies have been performed to identify phase and microstructural changes due to the welding process. The resultant distortion has then been measured by photogrammetric techniques and related to the experimental findings.

MATERIALS AND EXPERIMENTS

Rolled sheets, 4 mm in thickness, made of high strength low alloy ferritic-pearlitic steel, designated as grade DH-36, have been laser cut to form plates measuring 1000 × 500 mm. The nominal chemical composition of the steel plate is shown in Table 1. The butt welded sample was fabricated by metal inert gas (MIG) welding with NST MC-1 [1] weld wire, the composition of which is shown in Table 1. The weld wire has been chosen to over-match the plate's yield strength.

Table 1: Composition (wt%) of DH-36 steel [2] and the NST MC-1 weld wire [1].

	C	Si	Mn	P	S	Cu	Ni	Cr	Nb
Plate	0.11	0.181	1.29	0.014	0.004	0.023	0.029	0.025	0.013
Wire	0.07	0.609	1.421	0.012	0.011	0.137	0.035	0.021	0.017

Weld Fabrication and Thermal Data Acquisition

The plates being joined were held 4 mm apart by a series of tack welds and were rested, unrestrained on wooden pallets during the welding process. The welding power and speed were approximately 3150 W and 3.2 mms^{-1}, respectively. A single pass weld was made opposing the rolling direction.

Temperatures were monitored during the welding process by Type K thermocouples attached over a range of distances from the weld centre, at the mid length of the plate.

Neutron Diffraction Measurements

Neutron diffraction measurements were performed using the time-of-flight (TOF) method on the instrument ENGIN-X at the spallation source ISIS, UK. A schematic illustration of the instrument is shown in Figure 1, where the scattering vectors Q_1 and Q_2 define the measuring directions. The two detector banks are located at the Bragg angle, $2\theta_B = \pm 90$ °.

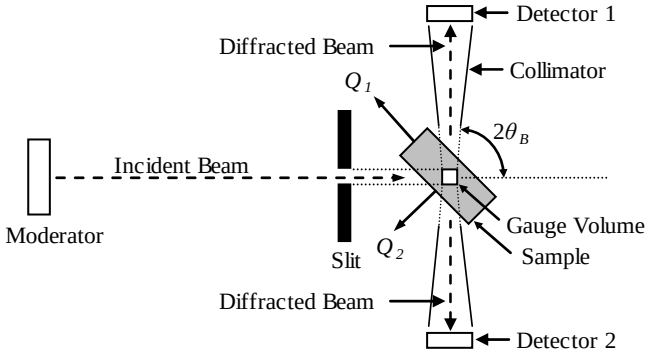

FIGURE 1: SCHEMATIC ILLUSTRATION OF THE DIFFRACTOMETER ARRANGEMENTS, AFTER [3].

The specimen was placed in two orientations to measure the strain in the longitudinal and transverse directions of the butt weld. A measurement of the strain in the direction normal to the plate surface was obtained twice, one from each orientation. A gauge volume was defined using a slit width of 1 mm and height of either 10 mm or 3 mm for the measurements in the transverse and longitudinal directions, respectively, and a gauge width of 1 mm was selected using the collimators (see Figure 2a and b).

For each orientation five sets of measurements were made through the thickness of the specimen, at the specimen's mid length along the weld, that were positioned at the nominal centre of the plate and at ± 0.65 mm and ± 1.30 mm from the plate centre. For each of these five positions through the plate thickness, the weld was traversed and measurements were taken at 45 points located between ± 100 mm from the weld centre.

Comb reference samples were manufactured from a butt welded plate which was nominally identical to that used for ND measurements. The comb was centered upon the weld and contained a total of 26 teeth of 40 mm in height with their long axes parallel to the welding direction. The comb teeth had a square (2 × 2 mm) cross-section and were equispaced with a centre to centre distance of 4 mm. This enabled the strain free lattice parameters to be measured at various distances from the weld centre. The comb was orientated to measure the lattice parameters in both the transverse and longitudinal direction using a gauge width of 1 mm and slit height and width of 10 mm and 1 mm, respectively, in both cases.

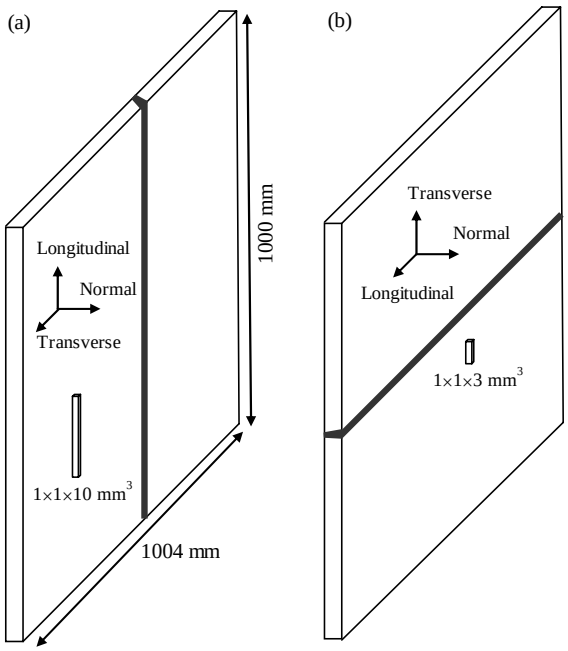

FIGURE 2: SCHEMATIC ILLUSTRATION OF SPECIMEN SET UP FOR (a) TRANSVERSE AND (b) LONGITUDINAL DIRECTION MEASUREMENTS, DEFINING GAUGE VOLUME

To examine any effects of manufacturing and laser cutting, measurements have been performed on an unwelded base plate. Measurements were taken at the mid height (500 mm) in three orthogonal directions corresponding to the longitudinal and transverse directions of the butt welded plate and normal to the plate surface. Measurements were obtained at 1 mm intervals from 1 mm away from the plate surface and extending 13 mm into the plate width, using a gauge width of 1 mm and slit height and width of 1.5 mm and 1 mm, respectively.

Data Analysis

A Rietveld analysis [4] can be performed on the entire diffraction pattern measured at the TOF source to determine the lattice parameter, a. Strain in a specific direction is given by

$$\varepsilon = \frac{a - a_0}{a_0} \qquad (1)$$

where a_0 is the lattice parameter measured in a strain free sample of the material. The uncertainty in the strain can be calculated as specified in [5].

When strains have been measured in three mutually orthogonal directions the direct stresses, σ_1, σ_2 and σ_3 can be determined from

$$\sigma_i = \frac{E}{1+\nu}\varepsilon_i + \frac{\nu E}{(1+\nu)(1-2\nu)}(\varepsilon_1 + \varepsilon_2 + \varepsilon_3) \qquad (2)$$

where i is the direct stress index, E and ν are the bulk elastic modulus and Poisson's ratio, respectively. Under certain conditions, a plane stress condition may be assumed, in which case one of these stresses, say σ_3 , is zero and Eqn (2) reduces to

$$\sigma_1 = \frac{E}{1-\nu^2}(\varepsilon_1 + \nu\varepsilon_2) \;;\; \sigma_2 = \frac{E}{1-\nu^2}(\varepsilon_2 + \nu\varepsilon_1) \qquad (3)$$

Distortion Measurements by Photogrammetry

The quantification of distortion through a body due to a fabrication process such as welding is critical to establish its cause, allowing process re-engineering to minimize the resulting distortion [6]. An image based method known as 'Multi Station Convergent Photogrammetry' has been employed to quantify the extent of distortion in the butt welded plate. This technique requires a network of intersecting images for the identification of common points within those images. This process can be carried out automatically using a series of coded targets, known as 'control points', whose co-ordinate positions in space (x,y,z) are known.

The plate was prepared by attaching a total of a hundred and ten retro reflective targets onto its surface to form a grid pattern, as seen in Figure 3. A target spacing of 100 mm has been used to describe the plate's topology. A target diameter of 6 mm has been used, which was estimated to be the optimum value in a previously simulated network [7]. A total of 12 control points have been located around the plates periphery to create a test field large enough to measure the 1 × 1 m butt welded plate, as shown in Figure 3. These control points, provide a known area of space with known co-ordinates and need to be regularly spaced around the object to ensure an even measurement field. Images have been collected from each side and corner of the control area from an elevated location to reduce the obliqueness of the view. At each location the camera was rotated to collect both a portrait and landscape image at each exposure location. Thus a network of 16 images was observed in total.

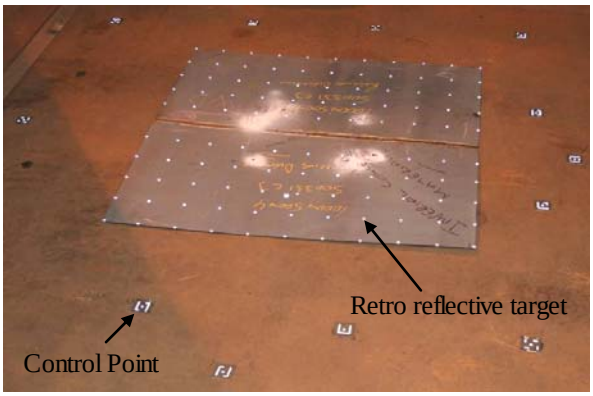

FIGURE 3: TEST FIELD FOR PHOTOGRAMMETRIC MEASUREMENTS

The imagery was processed into a format recognized by the distortion measurement software 'Vision Metrology Systems' (VMS) [8]. The camera was initially calibrated in order to account for the distortion inherent in the lens. Then, the known co-ordinates of the control points in each image were used to

automatically measure the image co-ordinates of the retro reflective targets. Using the 16 images an iterative procedure is performed to find the best solution to the co-ordinates of each target. Statistical measures of the precision of these results are provided by the software.

Metallographic and Hardness Investigations

Hardness studies can indicate the metallurgical changes caused by welding. A Vickers hardness survey has been performed along a cross-section of the butt welded plate within the fusion zone, heat affected zone (HAZ) and parent material (PM) using a 10 kg force.

The nominally identical butt welded plate to that used for ND measurements has been sectioned to examine the macro and microstructure of the weld cross-section. Specimens were cut using a flood lubricant, mounted and wet ground on SiC papers up to a Grade 4000, then polished using diamond paste, down to 1 μm, and Al_2O_3 emulsion. Subsequently the specimens were ultrasonically cleaned and lightly etched using 3% Nital solution. A bright field transmission-electron microscopy image (BF-TEM) has been produced from thin foil specimens to enable a microstructural analysis of the HAZ.

RESULTS AND DISCUSSION

Thermal Distributions

A typical thermal profile measurement at approximately 12 mm from the weld centre is shown in Figure 4. The weld torch traversed the plate in the first 315 s. A peak temperature of 475 °C is recorded at this location.

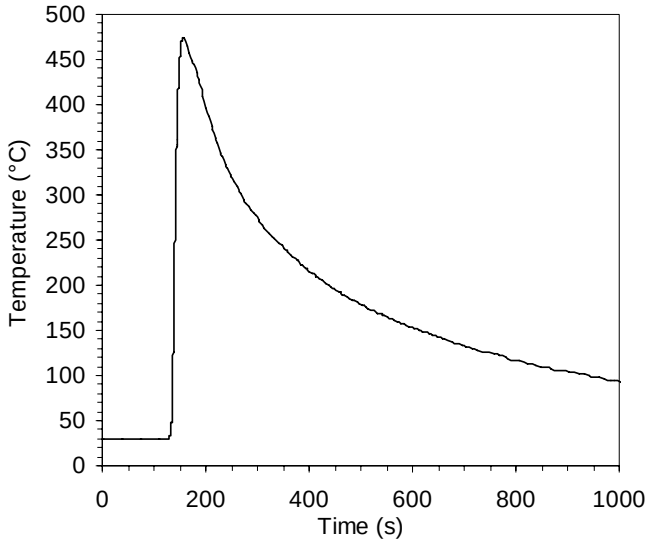

FIGURE 4: TYPICAL THERMAL PROFILE MEASUREMENT

Metallographic and Hardness Studies

A macrograph of the weldment is shown in Figure 5, where the fusion zone, HAZ and parent material (PM) regions are indicated. The weld extends a distance of approximately 4.5–6 mm from weld centerline. A HAZ 5–7 mm in width is observed and hence the undisturbed PM is seen at distances of over 10 mm from the weld centre.

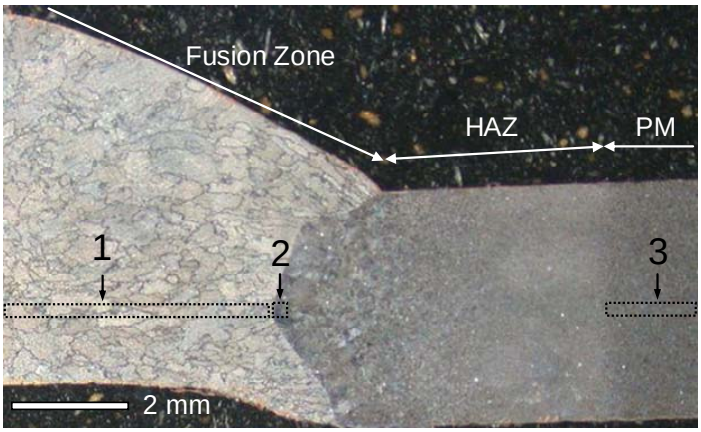

FIGURE 5: MACROGRAPH OF WELDED REGION

Three regions have been identified in Figure 5, (1) the fusion zone, (2) a region of the HAZ close to the fusion boundary and (3) the parent material. Optical (left) and secondary-mode scanning electron (right) micrographs of each region are shown in Figure 6. Proeutectoid ferrite was observed at the prior austenite grain boundaries of the fully transformed solidification microstructure while the remainder of the prior austenite grains consisted of interlocked acicular ferrite and pearlite. The prior austenite grain size were ~ 500 μm long and 100 μm wide. The acicular ferrite with cementite can be seen on the RHS of Figure 6 (a), where pores and non-metallic particles are also observed.

Close to the fusion boundary, Figure 6(b), a transformed bainitic microstructure is observed. The distribution of cementite precipitates between the ferrite platelets in upper bainite can be seen on the RHS of Figure 6(b) where a lath morphology is clearly observed. The typical ferritic-pearlitic microstructure of the parent material is shown in Figure 6(c). Partly spherodised cementite is seen in this region which is unaffected by the welding process. Though not clearly seen on the LHS of Figure 6(c), the pearlite is banded in the rolling direction. Ferrite grains of up to 40 μm in size have been found and the pearlite grains size is around 15 μm.

The presence of upper bainite in the HAZ, with the characteristic sheaf morphology observed in Figure 6(b), has been confirmed by BF-TEM, Figure 7. Dark carbide precipitates are clearly visible between the sheaves of ferrite platelets.

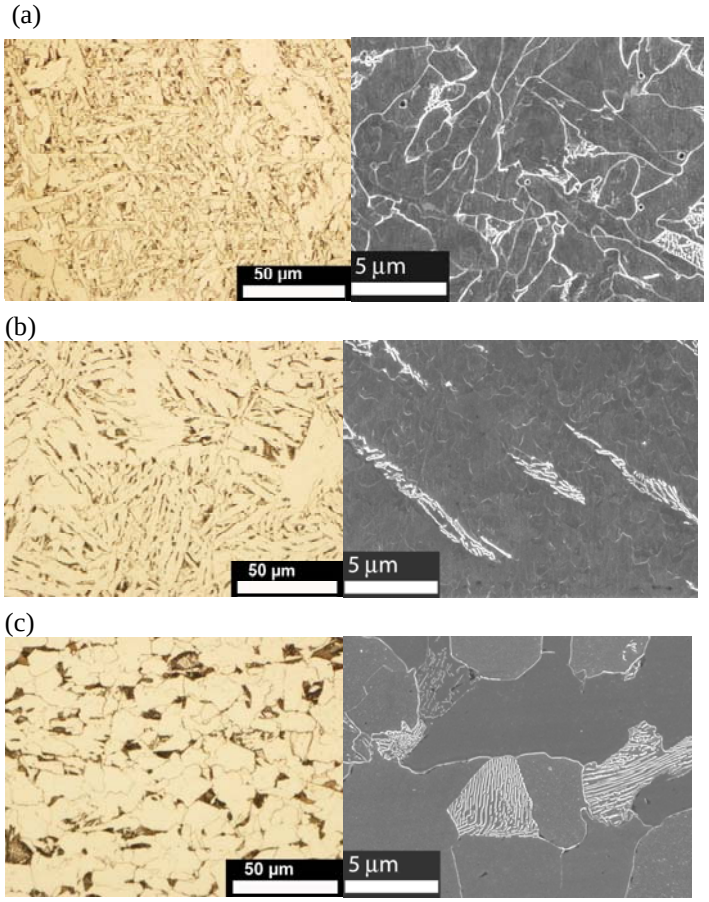

FIGURE 6: OPTICAL MICROGRAPHS AND FEGSEM IMAGES OF THE (a) FUSION ZONE (b) HAZ AND (c) PARENT MATERIAL

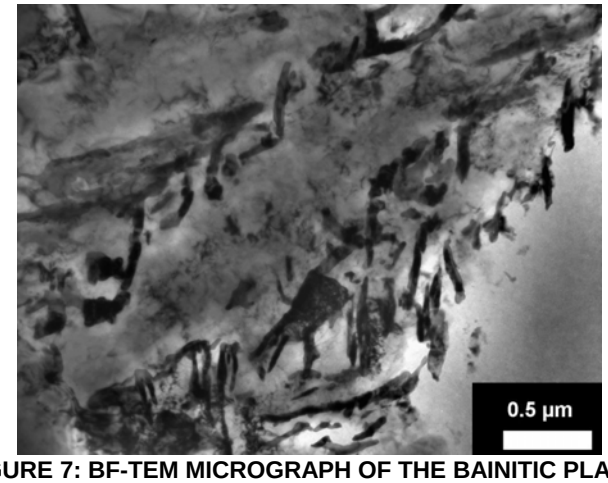

FIGURE 7: BF-TEM MICROGRAPH OF THE BAINITIC PLATES

The variation in the average Vickers hardness with position from the weld centre is shown in Figure 8, where the approximated location of the HAZ is indicated. The error bars shown indicate the standard deviation for the data. The hardness of the fusion zone and HAZ are comparable at around 190 HV and the PM is approximately 10% softer (170 HV) than the fusion zone and HAZ.

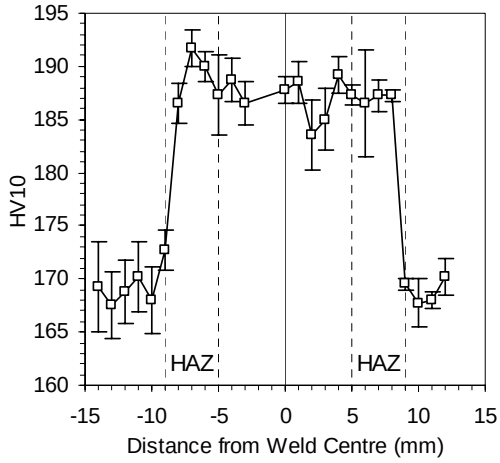

FIGURE 8: VICKERS HARDNESS VALUES

Residual Strain and Stress Distributions

The variation in the strain free lattice parameter values, a_0, measured in the comb in the three orthogonal directions, are shown in Figure 9 plotted against distance from the weld centreline.

Within the range of data scatter and experimental error no clear trend in a_0 can be determined with position from the weld centre in the three directions. The values in the three directions fall within the same scatter band. Therefore, a single a_0 value has been used for all directions and positions in the butt welded plate which is taken to be the average value for the data set and is equal to 2.8672 Å. The error in a_0, which is taken to be the standard deviation of the data set, is 9.93×10^{-5} Å.

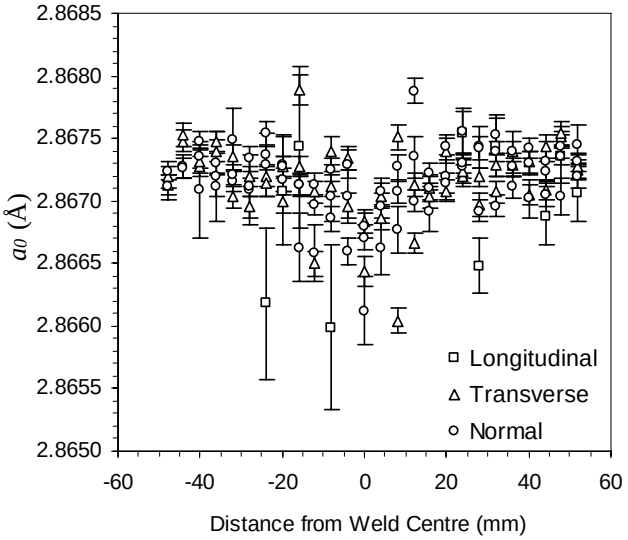

FIGURE 9: VARIATION IN THE MEASURED a_0 VALUES

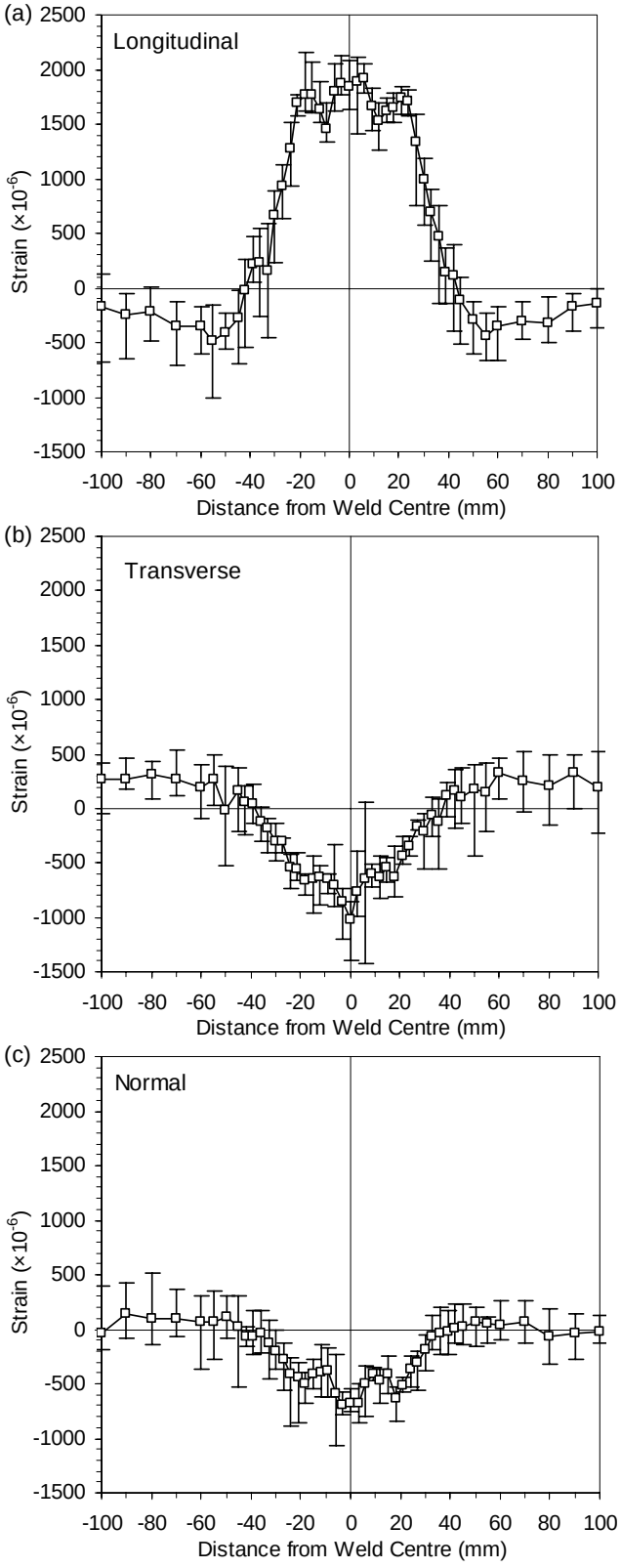

FIGURE 10: RIETVIELD-REFINED STRAINS MEASURED IN THE BUTT WELDED PLATE IN THE (a) LONGITUDINAL (b) TRANSVERSE AND (c) NORMAL DIRECTION

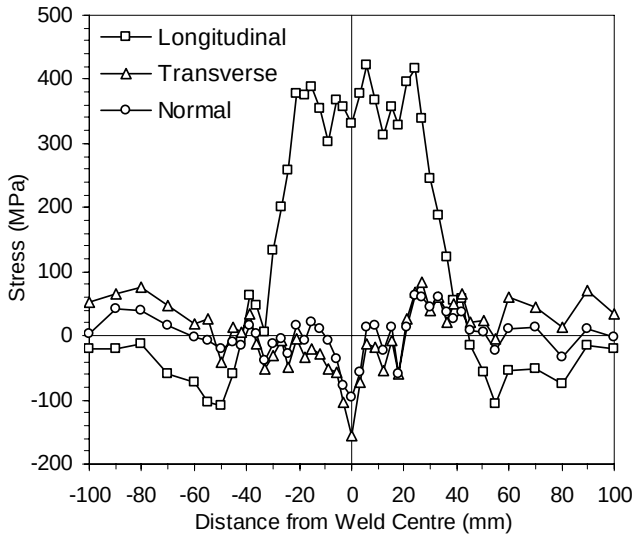

FIGURE 11: RIETVIELD-REFINED STRESS MEASUREMENTS IN THE THREE ORTHOGONAL DIRECTIONS WITHIN THE BUTT WELDED PLATE

The through thickness averages of the five sets of Rietveld-refined lattice strains measured at each position from the weld centre line in the butt welded plate have been calculated and are shown in Figure 10. The strain in the normal direction, shown in Figure 10(c), is the average of the two results associated with the measurements in the transverse and longitudinal directions. Error bars are used in Figure 10 to indicate the maximum range in values measured through the thickness of the plate. The corresponding residual stresses in the butt welded plate, determined using Eqn (2), are shown in Figure 11. The typical error calculated in each individual stress measurement was on the order of 16–20 MPa. The strain and stress distributions are approximately symmetric about the centre of the weld. The peak tensile/compressive stresses and strains are at the weld centre, which are on the order of the yield strength of this material, 441 MPa [2]. At approximately 10 mm from the weld centre a trough in the longitudinal strain is observed, which is attributed to the increased strain experienced in this region that may be caused by a phase transformation.

Effects of Plate Manufacture and Laser Cut

The Rietveld-refined strain and corresponding stress measurements in the base plate prior to welding are shown in Figure 12 and Figure 13, respectively. No significant stresses are expected to be present away from the plate edge; thus strain free lattice parameters were chosen for each measurement direction such that the stress 7 to 11 mm from the plate edge was, on average, equal to zero. At the plate surface a tensile strain of approximately 1130×10^{-6} is observed in the longitudinal direction, which is over half the maximum value observed in the butt weld (Figure 10a). In the transverse direction a compressive residual strain of approximately 1330×10^{-6} is seen, which is greater than the maximum compressive strain at the centre of the butt weld (Figure 10a). Generally there are no strains in the

normal direction or at distances greater than approximately 3 mm from the plate edge, in any direction.

Plane stress conditions have been assumed in the unwelded plate. Therefore only the transverse and longitudinal stresses, which were obtained using Eqn (3), are shown in Figure 13. A tensile stress of 230 MPa is found at the plate surface which diminished to approximately zero at distances over 2 mm from the edge. The peak compressive stress in the transverse direction, of approximately 90 MPa, is observed at a small distance from the plate edge. The plate edge is a free surface and hence the transverse stress is expected to diminish at this position. A compressive residual stress of 64 MPa is found within the volume sampled average of 0.5 mm from the plate edge, when plane stress conditions are assumed.

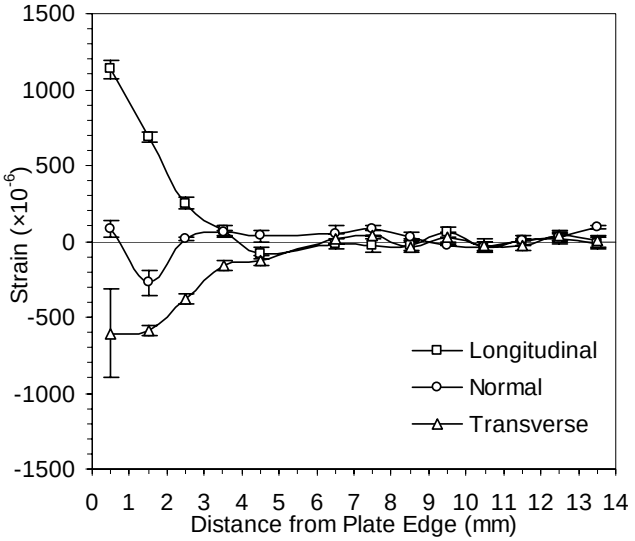

FIGURE 12: RIETVIELD-REFINED STRAIN MEASURMENTS IN THE UNWELDED BASE PLATE

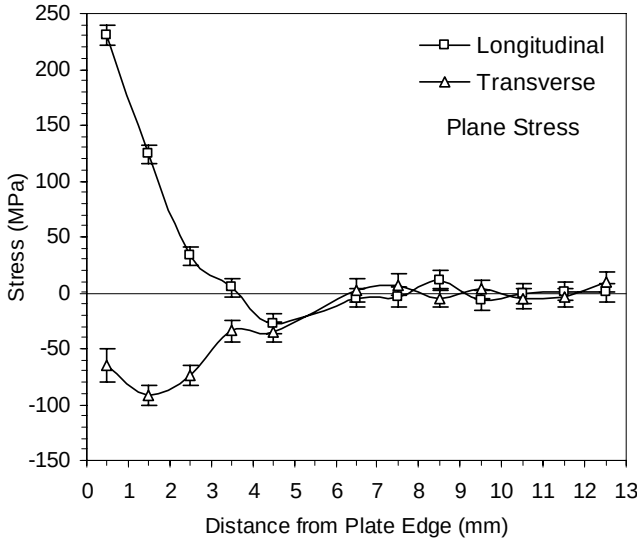

FIGURE 13: RIETVIELD-REFINED STRESS MEASURMENTS IN THE UNWELDED PLATE

Comparing Figure 11 and Figure 13 it can be seen that the peak stresses in the longitudinal and transverse directions of the base plate are approximately 50–60% of that found in the butt weld. The residual stresses and strains from the laser cut, though not insignificant close to the edge of the plate, diminish completely at distances of over 4 mm from the plate edge. However, high stresses and strains are observed for distances of over 20 mm from the centre of the butt weld in Figure 10 and Figure 11. Therefore the effects of the laser cut on the residual stresses observed in the butt weld are considered negligible.

Distortion Measurements by Photogrammetry

A 3-D contour plot of the distortion measured on the plate's surface is shown in Figure 14. In this figure the *x* co-ordinate indicates the distance along the length of the plate in the longitudinal direction, the *y* co-ordinate is transverse to the weld and the *z* co-ordinate is normal to the plate's surface. The weld centerline is thus located along the middle of the *y* axis (y = 500 mm). The weld pass started at the position x = 1000 mm and ran to x = 0 mm. Note that there are no distortion data in the weld itself. The resulting network indicated a precision of 1:210000 of the object size has been achieved with an average precision of 0.01 mm in *x*, *y* and *z* for all targets.

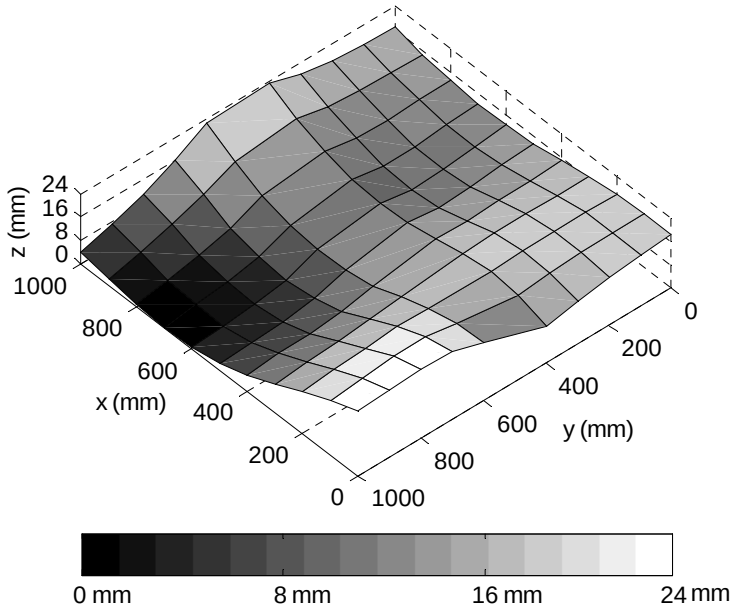

FIGURE 14: DISTORTION TOPOLOGY OF PLATES SURFACE

As can be seen in Figure 14, an unsymmetrical profile has resulted from the welding process. The largest out of plane displacement has occurred near the corner of the plate, at the co-ordinates (0, 800), where a *z* co-ordinate position of 23.4 mm is measured relative to the lowest position on the plate.

The asymmetric nature of the distortion is emphasized in Figure 15(a), where the relative *z* coordinate of each measurement position along the length of the plate edges (in the longitudinal direction), i.e. at y = 0 and 1000 mm, is plotted as a function of *x* co-ordinate. For a given *x* position a maximum

difference of 13.5 mm is observed in the relative displacement of both edges. At the midlength of the plate, x = 500 mm, the displacement generally decreases as the plate is transversed in the positive y direction. As illustrated in Figure 15(b), this decrease appears to be approximately linear except for in the vicinity of the weld, the centre of which is positioned at y = 500 mm, where an increase in distortion is experienced. Note that an interpolation has not been made here between the co-ordinates y = 400 and 600 mm as the weld is located between these two points. Both plate edges (y = 0 and 1000 mm) have a relative displacement of 11 mm at the midlength of the plate (x = 500 mm).

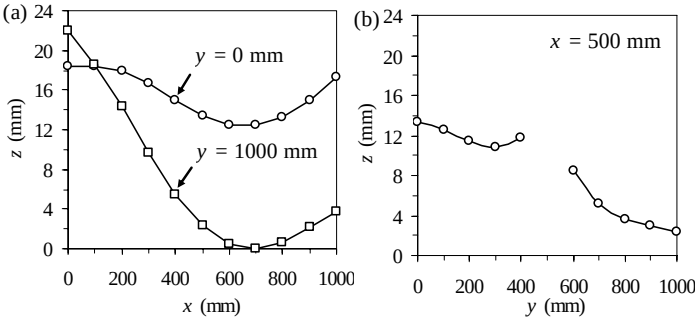

FIGURE 15: DISTORTION PROFILE (a) LONGITUDINALLY AT THE PLATE EDGES (b) ACROSS THE PLATE'S MIDLENGTH

CONCLUSIONS

The minimum thickness of ship panels may be limited by the extent of welding distortion exhibited during their manufacture. Residual stress and distortion measurements resulting from the butt welding of two large plates measuring 1 × 0.5 m and only 4 mm in thickness of grade DH-36 ferritic-pearlitic steel have been reported together with an examination of the weldment's microstructure through metallographic and hardness studies. Optical and field emission gun scanning electron microscope (FEGSEM) micrographs have revealed the presence of bainite in the HAZ, which was further confirmed through bright field transmission electron microscope (BF-TEM), proving that a phase transformation has taken place. It has therefore been established that modeling of the welding process will require consideration of phase transformations in the weld and HAZ. A Rietveld-refined analysis has been performed on the neutron diffraction (ND) measurements. The peak residual stresses, located at the weld centre, are found to be close to the material's yield stress. A trough in the longitudinal strain is observed at approximately 10 mm from the weld centre, which is thought to be attributed to phase transformations. Neutron diffraction measurements on an unwelded plate have revealed residual stresses, on the order of half the yield stress, at the plate edge, believed to be due to the laser cutting process. This stress rapidly diminishes at very small distances from the plate edge which, after the welding process, have been found to form part of the fusion zone. A 3-D map of the resultant distortion has been obtained using photogrammetry. An unsymmetrical configuration of the plate's surface distortion has been observed. The relative out of plane displacement of all positions measured attained a maximum value of 23.4 mm.

These analyses will enable finite element models to be verified, with the aim of using the FE results to train artificial neural networks for the optimization of welding parameters to minimize weld distortion. Further *in situ* instrumented testing is required to maximize data availability for verification purposes and to examine the variation in nominally identical tests. The influence of the welded stiffeners and weld sequencing effects will also be examined in future work.

ACKNOWLEDGMENTS

The authors would like to thank employees at BAE Systems-Surface Fleet Solutions, Govan for their assistance and ENGIN-X at ISIS, UK for the provision of neutron beam time. This work is funded by the EPSRC grant number EP/D060729/1.

REFERENCES

1. Røed, E., *Certified Material Tests Report*, Norsk Sveiseteknikk AS, Norway, 15/02/2006, Personal Communication.
2. Lexhas, V., *Inspection Certificate*, DUFERCO CLABECQ SA, Belgium, Certificate Number ANT : 0500001/474, 20/10/2006, Personal Communication.
3. Santisteban, J.R., et al., *ENGIN-X: a third-generation neutron strain scanner.* Journal of Applied Crystallography, 2006. **39**: p. 812–825.
4. Von Dreele, R.B., J.D. Jorgensen, and C.G. Windsor, *Rietveld Refinement with Spallation Neutron Powder Diffraction Data.* Journal of Applied Crystallography, 1982. **15**: p. 581–589
5. Webster, G.A., Ed., *Polycrystalline Materials — Determinations of residual Stresses by Neutron Diffraction*. 2001, ISO/TTA3 Technology Trends Assessment: Geneva.
6. Johnson, G.W., et al. *Dimensional & Accuracy Control Automation In Shipbuilding Fabrication: An Integration Of Advanced Image Interpretation, Analysis, And Visualization Techniques*. in *ISPRS 2004 Congress XX*. 2004. Istanbul, Turkey.
7. Maas, H.H.-G., *Digital close-range photogrammetry for dimensional checking and control in a shipyard.* Proceedings of SPIE--the international society for optical engineering, 1994. **2350**: p. 108-114.
8. Goldan, M.M., *As-built product modeling and reverse engineering in shipbuilding through combined digital photogrammetry and CAD/CAM technology.* Journal of ship production, 2003. **19**(2): p. 98-104.